Journal of Applied Electrochemistry **31**: 437–443, 2001.

Anodic oxidation of nitric oxide on Au/Nafion®: Kinetics and mass transfer

J.-S. DO* and K.-J. WU
Department of Chemical Engineering, Tunghai University, Taichung, Taiwan 40704, ROC
*(*author for correspondence)*

Received 8 February 2000; accepted in revised form 3 October 2000

Key words: anodic oxidation, Au/Nafion®, kinetics, mass transfer, nitric oxide

Abstract

The rate determining step for the anodic oxidation of nitric oxide on Au/Nafion® was experimentally and theoretically found to be

$$NO + Au \rightarrow Au\text{–}NO_{(ads)}$$

The anodic oxidation of nitric oxide was first order with respect to nitric oxide. The reaction rate constant increased from 3.3×10^{-5} to 9.6×10^{-5} cm s^{-1} as the applied potential increased from 0.74 to 0.77 V. The anodic oxidation of nitric oxide was controlled by the electrochemical kinetics when the anodic potential was less than 0.8 V. When the potential was greater than 1.0 V, it was located in the mass transfer region. The limiting current increased from 1184 to 1589 μA with increase in gas flow rate from 250 to 750 ml min^{-1} when the potential was set at 1.05 V and the concentration of nitric oxide was 100 ppm. The diffusion resistance in the gas diffusion layer can be neglected for gas flow rates greater than 750 ml min^{-1}. The diffusivity of nitric oxide and the equivalent diffusion layer thickness within the porous electrode were evaluated to be 3.43×10^{-4} cm^2 s^{-1} and 0.051 cm, respectively.

List of symbols

A	surface area of anode (cm^2)
C	concentration (mol cm^{-3})
D	diffusivity (cm^2 s^{-1})
F	faradaic constant (C mol^{-1})
I	current (A)
k	rate constant (cm s^{-1})
K	equilibrium constant
L	film thickness (cm)
N	number of electrons transferred
r	reaction rate (mol s^{-1} cm^{-2})
t	time (s)
V	anodic potential (V)

Subscripts

app	applied
eff	effective
eq	equivalent
g	gas phase
L	limiting

Superscripts

m, n, p reaction orders

Greek symbols

θ	adsorption fraction of anode

1. Introduction

Nitric oxide from combustion processes reacts with ozone to form nitrogen dioxide. This reaction causes a decrease in ozone levels in the atmosphere. Nitrogen dioxide also combines with water in the air to form nitrous and nitric acids resulting in acid rain. Hence, the development of gas sensors for monitoring the concentration of nitric oxide is very important.

Chemiluminescene [1] and electrochemical methods [2–12] have previously been used to analyze the concentration of nitric oxide in the gas phase. Electrochemical methods for monitoring the concentration of nitric oxide use three types of sensors: the conductimetric [2–3], potentiometric [4] and amperometric [5–12]. The metal oxides Al_2O_3, V_2O_5, SnO_2, ZnO and TiO_2 have all been used as sensing materials in conductimetric nitric oxide sensors [2, 3].

A good correlation between the experimental data and the theoretical equation (Nernst equation) has been found in the range of $10^3 \sim 10^4$ ppm nitric oxide when Pt and Ag^+–β-Al_2O_3 are used as the working electrode and solid

electrolyte in a potentiometric sensor [4]. However, the accuracy of the correlation is reduced when the concentration of nitric oxide is less than 1000 ppm [4].

The sensitivities of amperometric nitric oxide gas sensors based on a Au/C gas diffusion electrode were found to be 7.8 μA $(ppm)^{-1}$ [5] and 9.0 μA $(ppm)^{-1}$ [7–9], respectively. In addition, gas sensors based on solid polymer electrolytes have been widely used to detect the concentrations of various gases [11]. The sensitivity and detection limit of a silicon micro amperometric NO gas sensor using Au/Nafion® as the working electrode were found to be 0.03 μA $(ppm)^{-1}$ and 5 ppm, respectively [10]. Au/SPE (solid polymer electrolyte) prepared by the chemical plating method has been used as the working electrode for an amperometric nitric oxide gas sensor [12]. The preparation and characteristics of Au/SPE and the sensing behaviour of an amperometric nitric oxide gas sensor have been investigated [12].

Nitric oxide sensors based on SPE, such as Nafion®, have been widely used to detect the concentration of nitric oxide dissolved in aqueous solutions [13–18]. However, little research on amperometric nitric oxide gas sensors based on SPEs [10–12] has been reported. The kinetics of the anodic oxidation of nitric oxide on Au/SPE in the gas–solid system and the mass transfer of nitric oxide within the porous electrode are seldom mentioned in the literature. This work, investigates the kinetics of the anodic oxidation of nitric oxide on Au/Nafion® and the mass transfer of nitric oxide through the porous electrode.

2. Experimental details

2.1. *Preparation of Au/Nafion®*

Gold was plated onto a Nafion® membrane by the Takenaka–Torikai (T–T) chemical plating method [20]. The concentration of $AuCl_4^-$ in the chemical plating solution was analysed by atomic adsorption spectrophotometry (AAS). The Au loading on Nafion® was calculated from the difference between the initial and residual concentrations of $AuCl_4^-$ in the plating solutions.

2.2. *Anodic oxidation of nitric oxide*

Au/Nafion® was used both as a working electrode and as a separator for dividing the electrochemical cell into two chambers. The counter chamber, located at the backside of the Au/Nafion®, was filled with 0.5 M H_2SO_4 aqueous solution which provides protons and water for ionic conduction in the Nafion®. Platinum wire (0.5 mm dia., 5.0 cm length) and Ag/AgCl/3 M NaCl aqueous solution were used as the counter and reference electrodes, respectively. The test gases flowed into the working chamber and directly contacted the working electrode (Au). An Au O-ring, used as a current collector, was placed in contact with the working electrode. Two rubber O-rings were placed on either side of the Au/Nafion® to prevent leakage of the gas from the working chamber and that of aqueous solution from the counter chamber. The concentration of nitric oxide in the gas phase and the gas flow rate were controlled with a mass flow rate controller (Sierra 902C). The inlet gas was moisturized by passage through two vessels connected in series which contained one of the following saturated solutions: LiCl (22%), $Zn(NO_3)_2$ (49%), $Mg(NO_3)_2$ (61%), NaCl (82%), or pure water (100%); the numbers in parentheses specify the corresponding relative humidity (RH).

The relationship between the current and the potential was measured with an electrochemical analyser (BAS 100B). Au/Nafion® prepared by the chemical plating method was scanned in the potential range $0 \sim 1.8$ V (vs Ag/AgCl/3 M NaCl aqueous solution) for 1 h prior to measurements being performed. This procedure was carried out to stabilize the working electrode and to remove impurities from the electrode surface. The deviation of the current measured several times was found to be $\pm 1\%$.

3. Theoretical analysis

3.1. *Kinetics of anodic oxidation of nitric oxide*

When nitric oxide is transferred from the bulk phase to the anodic surface it is readily oxidized according to the following equation [6]

$$NO + 2\ H_2O \rightarrow HNO_3 + 3\ H^+ + 3\ e^- \tag{1}$$

The behaviour of the anodic oxidation of nitric oxide on Au is similar to that of anodic oxidation of carbon monoxide [5, 6]. Therefore, the reaction mechanisms for the anodic oxidation of nitric oxide on Au [19] is postulated to be

$$Au + NO \underset{k_{-1}}{\overset{k_1}{\rightleftharpoons}} Au\text{–}NO_{(ads)} \tag{2}$$

$$Au\text{–}NO_{(ads)} + H_2O \underset{k_{-2}}{\overset{k_2}{\rightleftharpoons}} Au\text{–}NO(OH)_{(ads)} + H^+ + e^- \tag{3}$$

$$Au\text{–}NO(OH)_{(ads)} + H_2O \underset{k_{-3}}{\overset{k_3}{\rightleftharpoons}} Au\text{–}NO(OH)_{2(ads)} + H^+ + e^- \tag{4}$$

$$Au\text{–}NO(OH)_{2(ads)} \underset{k_{-4}}{\overset{k_4}{\rightleftharpoons}} Au + HNO_3 + H^+ + e^- \tag{5}$$

Case 1

If Equation 2 is the rate-determining step, the reactions in Equations 3, 4 and 5 are under a pseudo-equilibrium

state. The net reaction rates in Equations 3, 4 and 5 are equal to zero.

$$\frac{r_2}{k_2} = \theta_{\text{Au–NO}}[\text{H}_2\text{O}] - \frac{k_{-2}}{k_2}\theta_{\text{Au–NO(OH)}}[\text{H}^+] = 0 \quad (6)$$

$$\frac{r_3}{k_3} = \theta_{\text{Au–NO(OH)}}[\text{H}_2\text{O}] - \frac{k_{-3}}{k_3}\theta_{\text{Au–NO(OH)}_2}[\text{H}^+] = 0 \quad (7)$$

$$\frac{r_4}{k_4} = \theta_{\text{Au–NO(OH)}_2} - \frac{k_{-4}}{k_4}\theta_{\text{Au}}[\text{HNO}_3][\text{H}^+] = 0 \quad (8)$$

where r is the reaction rate, θ_x is the adsorption fraction of substance x on the anode, and θ_{Au} is the fraction of anodic surface that does not adsorb any species. The summation of all θ_s is equal to unity.

$$\theta_{\text{Au}} + \theta_{\text{Au–NO}} + \theta_{\text{Au–NO(OH)}} + \theta_{\text{Au–NO(OH)}_2} = 1 \quad (9)$$

Since Equation 2 is assumed as the rate determining step, the rate of anodic oxidation of nitric oxide on Au can be expressed as

$$r_1 = k_1\theta_{\text{Au}}[\text{NO}] \quad (10)$$

The value of θ_{Au} can be obtained by solving Equations 6 to 9 simultaneously

$$\theta_{\text{Au}} = \frac{1}{1 + \frac{[\text{HNO}_3][\text{H}^+]}{K_4} + \frac{[\text{HNO}_3][\text{H}^+]^2}{K_3K_4[\text{H}_2\text{O}]} + \frac{[\text{HNO}_3][\text{H}^+]^3}{K_2K_3K_4[\text{H}_2\text{O}]^2}} \quad (11)$$

where $K_2 = k_2/k_{-2}$, $K_3 = k_3/k_{-3}$ and $K_4 = k_4/k_{-4}$. Substituting Equation 11 into Equation 10 yields the anodic nitric oxide oxidation rate as

$$r_1 = \frac{k_1[\text{NO}]}{1 + \frac{[\text{HNO}_3][\text{H}^+]}{K_4} + \frac{[\text{HNO}_3][\text{H}^+]^2}{K_3K_4[\text{H}_2\text{O}]} + \frac{[\text{HNO}_3][\text{H}^+]^3}{K_2K_3K_4[\text{H}_2\text{O}]^2}} \quad (12)$$

If a very low concentration of nitric oxide is introduced into the reaction system and nitric acid is not contained in the inlet stream, we can assume that

$$\frac{[\text{HNO}_3][\text{H}^+]}{K_4} \ll 1, \frac{[\text{HNO}_3][\text{H}^+]^2}{K_3K_4[\text{H}_2\text{O}]} \ll 1,$$
$$\frac{[\text{HNO}_3][\text{H}^+]^3}{K_2K_3K_4[\text{H}_2\text{O}]^2} \ll 1$$

Equation 12 can then be rewritten as

$$r_1 = k_1[\text{NO}] \quad (13)$$

Equation 13 indicates that the anodic oxidation of nitric oxide is first order with respect to nitric oxide.

Case 2

If Equation 3 is the rate determining step, the anodic oxidation rate can be expressed as

$$r_2 = k_2\theta_{\text{Au–NO}}[\text{H}_2\text{O}] \quad (14)$$

Similarly to case 1, the term, $\theta_{\text{Au–NO}}$, can be obtained as

$$\theta_{\text{Au–NO}} = \frac{K_1[\text{NO}]}{1 + K_1[\text{NO}] + \frac{[\text{HNO}_3][\text{H}^+]}{K_4} + \frac{[\text{HNO}_3][\text{H}^+]^2}{K_3K_4[\text{H}_2\text{O}]}} \quad (15)$$

where $K_1 = k_1/k_{-1}$. The anodic oxidation rate is obtained by substituting Equation 15 into Equation 14

$$r_2 = \frac{k_2K_1[\text{NO}][\text{H}_2\text{O}]}{1 + K_1[\text{NO}] + \frac{[\text{HNO}_3][\text{H}^+]}{K_4} + \frac{[\text{HNO}_3][\text{H}^+]^2}{K_3K_4[\text{H}_2\text{O}]}} \quad (16)$$

If the concentration of nitric oxide is very low in the inlet gas with the absence of nitric acid, Equation 16 can be simplified as

$$r_2 = k_2K_1[\text{NO}][\text{H}_2\text{O}] \quad (17)$$

Equation 17 indicates that the anodic oxidation rate is first order with respect to nitric oxide and water in the gas phase, respectively.

Case 3

Similarly, when the rate determining step is assumed to be Equation 4, the anodic oxidation rate of nitric oxide on Au is found to be

$$r_3 = k_3K_1K_2[\text{NO}][\text{H}_2\text{O}]^2/[\text{H}^+] \quad (18)$$

The reaction orders of the anodic oxidation of nitric oxide on Au are obtained from Equation 18 to be 1, 2 and −1 with respect to NO, H_2O and H^+, respectively.

Case 4

The anodic oxidation rate on Au can be expressed as Equation 19 when Equation 5 is assumed to be the rate determining step.

$$r_4 = k_4K_1K_2K_3[\text{NO}][\text{H}_2\text{O}]^2/[\text{H}^+]^2 \quad (19)$$

Equation 19 reveals that the reaction orders are 1, 2 and −2 with respect to NO, H_2O and H^+, respectively.

3.2. *Mass transfer of nitric oxide*

The mass transfer of nitric oxide from the bulk phase through the gas film and porous electrode is shown in Figure 1. The concentration of nitric oxide in the gas bulk phase is denoted as C^*, which decreases to C' when nitric oxide diffuses through the gas film (L_g) to the gas–electrode interface. The porous Au anode is assumed to have an equivalent thickness, L_{eq}. The anodic oxidation of nitric oxide then occurs at an electroactive surface located at the inside of the porous electrode. The concentration of nitric oxide is depleted from C' to C_s when nitric oxide transfers through the porous electrode to the electroactive surface as proposed in this model.

When the limiting current (I_L) of anodic nitric oxide oxidation is applied, the mass flux of nitric oxide can be expressed as

$$J_{NO} = \frac{I_L}{nFA} = \frac{D_{eq}}{L_{eq}} C' = \frac{D}{L_g}(C^* - C') \tag{20}$$

where n is the number of electrons transferred in the anodic oxidation of nitric oxide, F is the faradaic constant (96 485 C mol^{-1}), A is the anodic surface area, D_{eq} is the equivalent diffusivity of nitric oxide in the porous Au anode, and D is the diffusivity of nitric oxide in the gas diffusion layer. Solving Equation 20 yields the concentration of nitric oxide in the gas-electrode interface (C') is

$$C' = \frac{DL_{eq}}{DL_{eq} + D_{eq}L_g} C^* \tag{21}$$

Substituting Equation 21 into Equation 20 gives the limiting current for the anodic oxidation of nitric oxide as

$$\frac{I_L}{nFA} = \frac{DD_{eq}}{DL_{eq} + D_{eq}L_g} C^* \tag{22}$$

4. Results and discussion

4.1. *Kinetics of the anodic oxidation of nitric oxide*

The uncompensated resistance between the working electrode and the reference electrode measured by the positive feedback method was found to be in the range 2.40–2.67 Ω. Because the current between the working and reference electrodes was small, the deviation in potential due to the uncompensated potential can be neglected.

Based on the analysis in the theoretical section, a general reaction rate equation for the anodic oxidation of nitric oxide on Au/SPE is

$$\frac{I}{nFA} = k\frac{[NO]^n[H_2O]^m}{[H^+]^p} \tag{23}$$

where n, m and p are the reaction orders with respect to NO, H_2O and H^+, respectively.

4.1.1. *Effect of the concentration of nitric oxide in the gas phase*

The anodic oxidation of nitric oxide is insignificant for potentials less than 0.70 V as shown in Figure 2. The current becomes significant until the potential is greater than 0.72 V. As indicated in Figure 2, the anodic oxidation of nitric oxide is under reaction control when the anodic potential is less than 0.80 V for various concentrations of nitric oxide. At potentials greater than 1.0 V, a limiting current for nitric oxide oxidation is observed. The reaction is then under mass transfer control.

Linear relationships for various potentials are obtained from a log(I/nFA) against log[NO] plot (Figure 3). The slopes of these lines show the reaction order with respect to nitric oxide at various potentials. The slopes obtained in the range 1.01–1.05 (Table 1) suggest the oxidation to be first order with respect to nitric oxide. Increasing the applied potential from 0.74

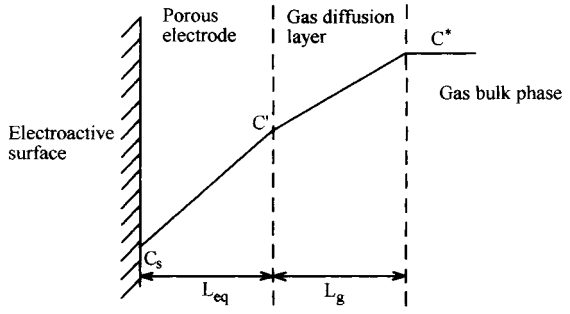

Fig. 1. Scheme of the mass transfer of nitric oxide from the gaseous phase to the anodic surface.

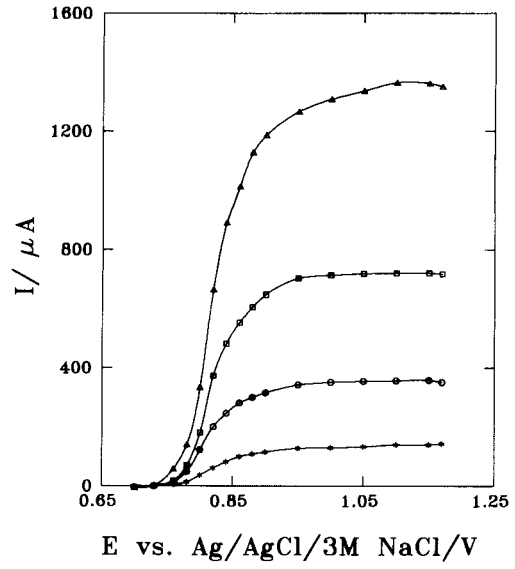

Fig. 2. The net I/E curves for various concentration of nitric oxide. Gas flow rate 45 ml min^{-1}; electrolyte 0.5 M H_2SO_4; $T = 30$ °C; geometric anodic area 0.5 cm^2; electroactive area of anode 200 cm^2; Au loading 7.5 mg cm^{-2}. [NO]: (∗) 100, (○) 250, (□) 500 and (△) 1000 ppm.

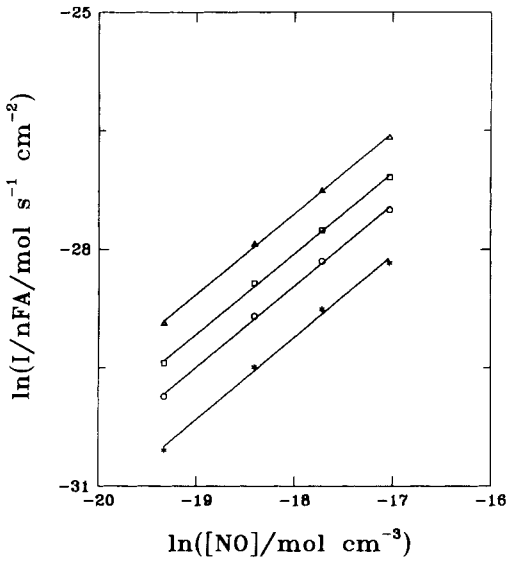

Fig. 3. Plot of $\ln(I/nFA)$ against $\ln([NO])$ for various applied potentials. Gas flow rate 45 ml min^{-1}; electrolyte 0.5 M H_2SO_4; $T = 30$ °C; geometric anodic area 0.5 cm^2; electroactive area of anode 200 cm^2; Au loading 7.5 mg cm^{-2}. V_{app}: (∗) 0.74, (○) 0.75, (□) 0.76 and (△) 0.77 V.

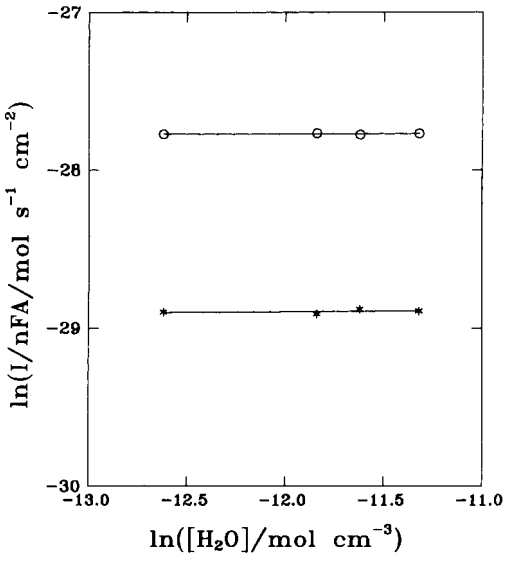

Fig. 4. Plot of $\ln(I/nFA)$ against $\ln([H_2O])$ for various applied potentials. [NO] = 500 ppm; gas flow rate 45 ml min^{-1}; electrolyte 0.5 M H_2SO_4; $T = 30$ °C; geometric anodic area 0.5 cm^2; electroactive area of anode 200 cm^2; Au loading 7.5 mg cm^{-2}. V_{app}: (∗) 0.73 and (○) 0.76 V.

to 0.77 V increases the reaction rate constant, as evaluated from the intercept of the lines in Figure 3, from 3.3×10^{-5} to 9.6×10^{-5} cm s^{-1} (Table 1).

4.1.2.*Effect of the water concentration in the gas phase*
At applied potentials of 0.73 and 0.76 V, the anodic current is approximately constant as the concentration of water increases from 3.3 to 12.1 mM. The slopes obtained from the linear plots of the $\log(I/nFA)$ against $\log[H_2O]$ at potentials of 0.73 and 0.76 V are 0.0018 and 0.0078, respectively (Figure 4). These results reveal that the reaction rate is independent of the water concentration in the gas phase. The reaction order with respect to water (m in Equation 23) is thus considered to be zero. According to the theoretical analysis, the reaction orders with respect to water in the gas phase are 1, 2 and 2 for cases 2, 3 and 4 (Equations 17, 18 and 19) in which Equations 3, 4 and 5 are assumed to be the rate determining step, respectively. In comparison with the theoretical analysis, the results suggest that the rate determining step is Equation 2 (i.e., the adsorption of nitric oxide onto the Au electrode) (case 1). The reaction rate on an Au electrode can then be expressed as

Table 1. Effect of potential on the rate constant of anodic oxidation of nitric oxide

V_{app} /V	Slope	Intercept	Rate constant (k) /cm s^{-1}
0.74	1.05	−10.3	3.3×10^{-5}
0.75	1.02	−10.0	4.5×10^{-5}
0.76	1.01	−9.9	5.2×10^{-5}
0.77	1.02	−9.3	9.6×10^{-5}

[NO] = 500 ppm; gas flow rate 45 ml min^{-1}; electrolyte 0.5 M H_2SO_4; $T = 30$ °C; geometric anodic area 0.5 cm^2; electroactive area of anode 200 cm^2; Au loading 7.5 mg cm^{-2}

$$\frac{I}{nFA} = k[NO] \tag{24}$$

where k is the rate constant of Equation 2 (k_1).

4.2. *Mass transfer of nitric oxide*

As described in the theoretical section and depicted in Figure 1, the resistance for mass transfer of nitric oxide from the bulk phase to electroactive surface results from mass transfer in the gas diffusion layer and diffusion in the porous electrode. In general, the gas diffusion layer thickness and the mass transfer resistance in the gas diffusion layer decrease with increase in mass flow rate [21–23]. Therefore, the gas diffusion rate and the limiting current increase with gas flow rate. Further increase in gas flow rate will eventually cause the mass transfer resistance in the gas diffusion layer to be negligible compared with that within the porous electrode. Finally, the effect of gas flow rate on the limiting current becomes insignificant.

Increasing the gas flow rate from 250 to 750 ml min^{-1} causes the limiting current to increase from 1184 to 1589 μA when the anodic potential and the concentration of nitric oxide are 1.05 V and 100 ppm, respectively (Figure 5). Further increasing the gas flow rate to 1000 ml min^{-1} leads to insignificant change in the limiting current. These results indicate that the mass transfer resistance can be neglected for gas flow rates greater than 750 ml min^{-1}.

The anodic current against run time was recorded for various gas flow rates when the anodic potential was switched from 0.45 to 1.05 V and the concentration of nitric oxide was 100 ppm. In the initial stages, a large

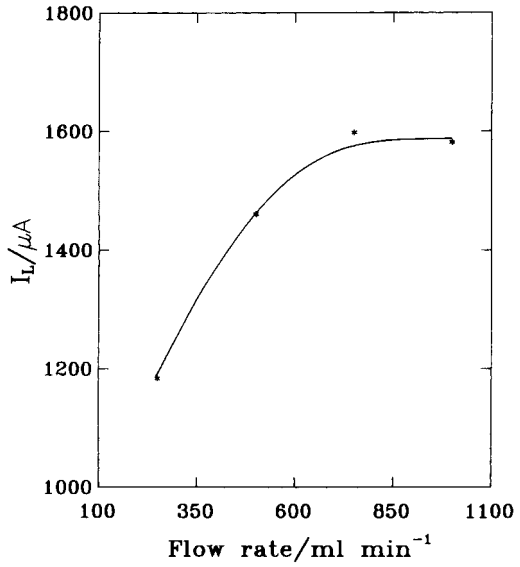

Fig. 5. Effect of gas flow rate on the limiting current of anodic oxidation of nitric oxide. [NO] = 100 ppm; electrolyte 0.5 M H_2SO_4; $T = 30$ °C; geometric anodic area 0.5 cm^2; electroactive area of anode 200 cm^2; Au loading 7.5 mg cm^{-2}.

anodic current was observed due to the high concentration of nitric oxide near the electroactive surface, as illustrated in Figure 6. The anodic current decreased with time due to the decrease in nitric oxide concentration at the anodic surface. Finally, a steady current was achieved when the mass transfer of nitric oxide through the gas diffusion layer and the porous electrode was equal to the consumption of nitric oxide by the anodic oxidation. The relationship between anodic current and time is described by the following equation [24].

$$I = \frac{nFAC^* D_{\text{eff}}^{1/2}}{(\pi t)^{1/2}} \tag{25}$$

where D_{eff} is the effective diffusivity.

Straight lines are obtained by plotting the anodic current against the square root of run time ($t^{1/2}$), as shown in Figure 7. The experimental data correlate well with Equation 25. The slopes of the straight lines are listed in Table 2. Substituting the values of n, F, A and C^* into the slope (column 2 in Table 2), $nFAC^* D_{\text{eff}}^{1/2}/\pi^{1/2}$, the effective diffusivities are calculated and listed in column 4 of Table 2. The effective diffusivity decreases from 2.96×10^{-3} to 3.49×10^{-4} cm^2 s^{-1} with increase in the gas flow rate from 0 to 750 ml min^{-1}. The effective diffusivity changes slightly when the gas flow rate is greater than 750 ml min^{-1}. The results in Table 2 and Figures 5 to 7 show that the diffusion resistance in the gas diffusion layer can be neglected and the effective diffusivity is mainly the diffusivity within the porous electrode when the gas flow rate is greater than 750 ml min^{-1}.

According to Fick's law, the current under steady state mass transfer condition is expressed as [24]

$$I = \frac{D_{\text{eff}}}{L_{\text{eff}}} nFAC^* \tag{26}$$

where L_{eff} is the effective diffusion layer thickness. Substituting the steady current shown in Figure 6, D_{eff} obtained in Table 2 and putting values of n, F, A and C^* into Equation 26, the effective diffusion layer thickness (L_{eff}) was calculated and listed in column 5 of Table 2. When the gas flow rate increases from 250 to 750 ml min^{-1}, L_{eff} decreases from 0.14 to 0.052 cm. By

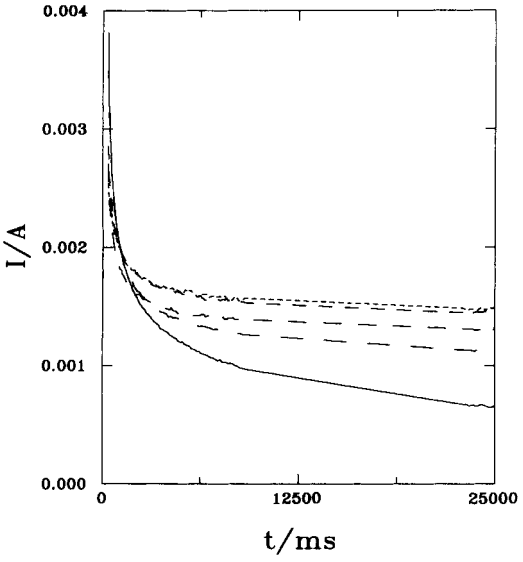

Fig. 6. Effect of run time on the current of anodic oxidation of nitric oxide for various gas flow rate. Potential step: 0.45 V → 1.05 V; [NO] = 100 ppm; electrolyte 0.5 M H_2SO_4; $T = 30$ °C; geometric anodic area 0.5 cm^2; electroactive area of anode 200 cm^2; Au loading 7.5 mg cm^{-2}. Flow rate: (——) 0, (- —) 250, (– —) 500, (— — —) 750 and (– – – –) 1000 ml min^{-1}.

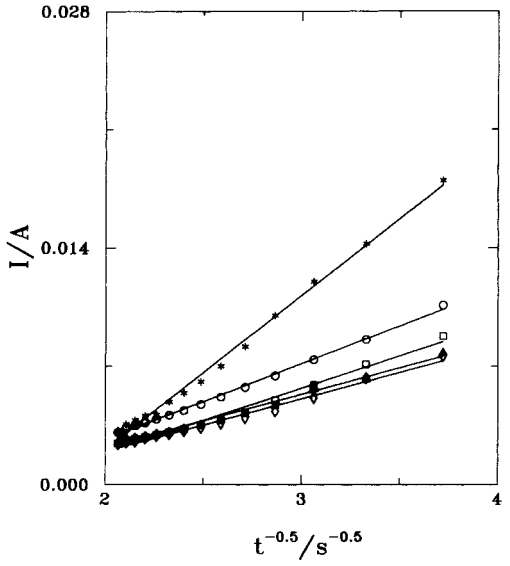

Fig. 7. Plot of I against $t^{-0.5}$ for various gas flow rate. Potential step: 0.45 V → 1.05 V; [NO] = 100 ppm; electrolyte 0.5 M H_2SO_4; $T = 30$ °C; geometric anodic area 0.5 cm^2; electroactive area of anode 200 cm^2; Au loading 7.5 mg cm^{-2}. Flow rate: (∗) 0, (○) 250, (□) 500, (△) 750 and (◆) 1000 ml min^{-1}.

Table 2. Effect of the gas flow rate on the effective diffusivity and diffusion layer thickness

Gas flow rate /ml min^{-1}	Slope	I_L /μA	D_{eff} /cm^2 s^{-1}	L_{eff} /cm
0	7.25×10^{-3}	–	2.96×10^{-3}	–
250	3.56×10^{-3}	1184	7.13×10^{-4}	0.14
500	3.03×10^{-3}	1461	5.17×10^{-4}	0.084
750	2.49×10^{-3}	1589	3.49×10^{-4}	0.052
1000	2.47×10^{-3}	1581	3.43×10^{-4}	0.051

Potential step: 0.45 V $\rightarrow$ 1.05 V; [NO] = 100 ppm; electrolyte 0.5 M $H_2SO_{4(aq)}$; T = 30 °C; geometric anodic area 0.5 cm^2; electroactive area of anode 200 cm^2; Au loading 7.5 mg cm^{-2}

further increasing the gas flow rate to 1000 ml min^{-1}, L_{eff} slightly decreases to 0.051 cm. The results also suggest that the diffusion resistance in the gas diffusion layer can be neglected for gas flow rates greater than 750 ml min^{-1}. The diffusivity of nitric oxide and the equivalent thickness of the diffusion layer (L_{eq}) in the porous electrode are found to be 3.43×10^{-4} cm^2 s^{-1} and 0.051 cm, respectively.

5. Conclusions

The anodic oxidation of nitric oxide on Au/Nafion® shows that the rate determining step is the adsorption of nitric oxide on the electroactive sites. The expression for the anodic oxidation current for nitric oxide was found to be

$$I = nFAk[\mathrm{NO}]$$

The rate constant k increased from 3.3×10^{-5} to 9.6×10^{-5} cm s^{-1} as the potential was changed from 0.74 to 0.77 V. The reaction rate for the anodic oxidation of nitric oxide is controlled by the electrochemical kinetics when the anodic potential is less than 0.80 V. At potentials greater than 1.0 V, a limiting current for the anodic oxidation of nitric oxide was observed and the reaction became mass transfer controlled. The diffusion resistance in the gas diffusion layer can be neglected and the overall diffusion resistance is mainly determined by the diffusion of nitric oxide within the porous electrode when the gas flow rate is greater than 750 ml min^{-1}. The diffusivity of nitric oxide and the equivalent thickness of the diffusion layer in the porous electrode were found to be 3.43×10^{-4} cm^2 s^{-1} and 0.051 cm, respectively.

Acknowledgement

The support of National Science Council of the Republic of China (NSC 85-2214-E-029-003) and Tunghai University is acknowledged.

References

1. A. Fontijn, A.J. Sabadell and R.J. Ronco, *Anal. Chem.* **42** (1970) 575.
2. T. Ishihara, K. Shiokawa, K. Eguchi and H. Arai, *Sensors and Actuators B* **19** (1989) 259.
3. S.C. Chang and D.B. Hicks, 'Tin Oxide Microsensors. Fundamentals and Applications of Chemical Sensor', Maple Press, New York, PA, (1986).
4. N. Rao, C.M. Bleek and J. Schoonman, *Solid State Ionics* **52** (1992) 339.
5. J.M. Sedlak and K.F. Blurton, *J. Electrochem. Soc.* **123** (1976) 1476.
6. J.M. Sedlak and K.F. Blurton, *Talanta* **23** (1976) 811.
7. K.F. Blurton and J.M. Sedlak, *US Patent 4 001 103* (1977).
8. K.F. Blurton and J.M. Sedlak, *US Patent 4 042 464* (1977).
9. K.F. Blurton and J.M. Sedlak, *US Patent 4 052 268* (1977).
10. F. Maseeh, M.J. Tierney, W.S. Chu, J. Joseph, H.-O.L. Kim and T. Otagawa, Transducers '91, International Conference on 'Solid State Sensors and Actuators', San Francisco, CA (1991), pp. 359–362.
11. F. Opekar and K. Stulik, *Anal. Chim. Acta* **385** (1999) 151.
12. J.S. Do and K.J. Wu, *Sensors and Actuators B* **67** (2000) 209.
13. F. Lantoine, S. Trevin, F. Bedioui and J. Devynck, *J. Electroanal. Chem.* **292** (1995) 85.
14. O. Raveh, N. Peleg, A. Bettleheim, I. Silbernman and J. Rishpon, *Bioelect. Bioenerg.* **43** (1997) 19.
15. F. Bedioui, S. Trevin, J. Devynck, F. Lantoin, A. Brunet and M.-A. Devynck, *Biosensors & Bioelectronics* **12** (1997) 205.
16. C. Privat, S. Trevin, F. Bedioui and J. Devynck, *J. Electroanal. Chem.* **436** (1997) 261.
17. J.-K. Park, P.H. Tran, J.K.T. Chao, R. Ghodadra, R. Rangarajan and N.V. Thakor, *Biosensors & Bioelectronics* **13** (1998) 1187.
18. M. Pontie, H. Lecture and F. Bedioui, *Sensors and Actuators B* **56** (1999) 1.
19. H. Kita and H. Nakajima, *Electrochim. Acta* **31** (1986) 193.
20. J.S. Do and R.Y. Shieh, *Sensors and Actuators B* **37** (1996) 19.
21. H. Schlichting, 'Boundary Layer Theory', McGraw-Hill, New York, (1955), pp. 204–206.
22. R. Bauer, D.K. Friday and D.J. Kirwan, *Ind. Eng. Chem. Fundam.* **20** (1981) 141.
23. T.C. Chou, J.S. Do, B.J. Hwang and J.J. Jow, *Chem. Eng. Comm.* **51** (1987) 47.
24. C. McCallum and D. Pletcher, *Electrochim. Acta* **20** (1975) 811.